Korean J. Chem. Eng., 37(6), 1008-1019 (2020)
DOI: 10.1007/s11814-020-0542-1

pISSN: 0256-1115
eISSN: 1975-7220

The influence of the Gemini surfactants hydrocarbon tail on in-situ synthesis of silver nanoparticles: Characterization, surface studies and biological performance

Samy M. Shaban[*,**,***] **and Dong-Hwan Kim**[*,**,†]

*School of Chemical Engineering, Sungkyunkwan University, Suwon 16419, Korea
**Biomedical Institute for Convergence at SKKU (BICS), Sungkyunkwan University, Suwon 16419, Korea
***Petrochemical Department, Egyptian Petroleum Research Institute (EPRI), Egypt
(*Received 19 December 2019 • accepted 13 March 2020*)

Abstract−Three different Gemini compounds containing different lengths of multi-carbonyl groups were synthesized, and the effect of their hydrocarbon tail length on the AgNPs synthesis was investigated. The Gemini surfactants with the long hydrocarbon chain tail produces small AgNPs with a narrow size distribution and high colloidal stability in an aqueous phase. The surface parameters of the aqueous solution were affected by the hydrocarbon chain length as well as phase temperature. The critical micelle concentration, assessed by surface tension and conductometric measurements, decreases with both increasing solution temperature and increasing hydrocarbon tail length. Thermodynamic calculations predicted the ability of the synthesized Gemini surfactant to adsorb on the phase surface and aggregate in a cluster.

Keywords: Multi-carbonyl Gemini Amphiphilic, Surface and Thermodynamic Parameters, AgNPs, Sulfate-reducing Bacteria, Emulsion Stability

INTRODUCTION

Surfactants are organic compounds composed of two parts with different polar properties. The surfactant head has an affinity to polar phases, while the tail is attracted to nonpolar phases. Surfactants are characterized by both an affinity for adsorption at interfaces and the tendency to form aggregates in clusters known as micelles [1,2]. Gemini cationic amphiphile includes two hydrophilic heads and two hydrocarbon tails, and the two heads are connected by either a rigid or flexible spacer [3-8]. Because of their structure, Gemini surfactants have superior biological, surface, and interfacial properties in comparison to conventional monomeric one that have only one hydrophilic part and one hydrophobic part. Their structure causes Gemini surfactants to have lower critical micelle concentrations (CMCs) [9-12], and higher wetting, solubilization, and foaming properties compared to conventional monomeric amphiphilic one. The specific chemical structure of Gemini surfactants enhances their tendency to produce a wide divergence of aggregate morphologies in solution [13-16].

Silver nanoparticles (AgNPs) show high catalytic and biological activity and can effectively eliminate pathogenic bacteria at low concentrations [17,18]. There are various techniques for the preparation of AgNPs, including photo-chemical and chemical reduction, thermal decomposition, micro-emulsion, and pulsed laser ablation. Most of these methods require surfactant compounds as stabilizing agents during preparation for controlling the nanoparticle size and morphology, which in turn determines the physical, chemical, optical, and catalytic properties of the produced nanoparticles [19-23]. Based on this, we investigated the effects of surfactant hydrocarbon tail length on size distribution, stability, and yield of the AgNPs. To date, only a few papers have discussed the effects of the surfactant hydrocarbon tail on nanoparticle size distribution [24,25].

The objective of this study was to synthesize multi-electronic rich Gemini cationic surfactants. The present research focuses on how the hydrophobic tail of surfactant play an essential role in controlling size, distribution, and amount of formed AgNPs throughout varying the total number of carbon atoms involved the double hydrophobic tail. The surface parameters of the prepared multi-electronic rich Gemini surfactants are studied temperature variation. The activities of the prepared amphiphiles as well as their colloidal AgNPs against pathogenic bacteria (Gram positive (G+) and negative (G−)), fungi, as well as sulfate reducing bacteria (SRB) are assessed to overcome increased microbial resistance.

MATERIALS AND METHODS

1. Materials

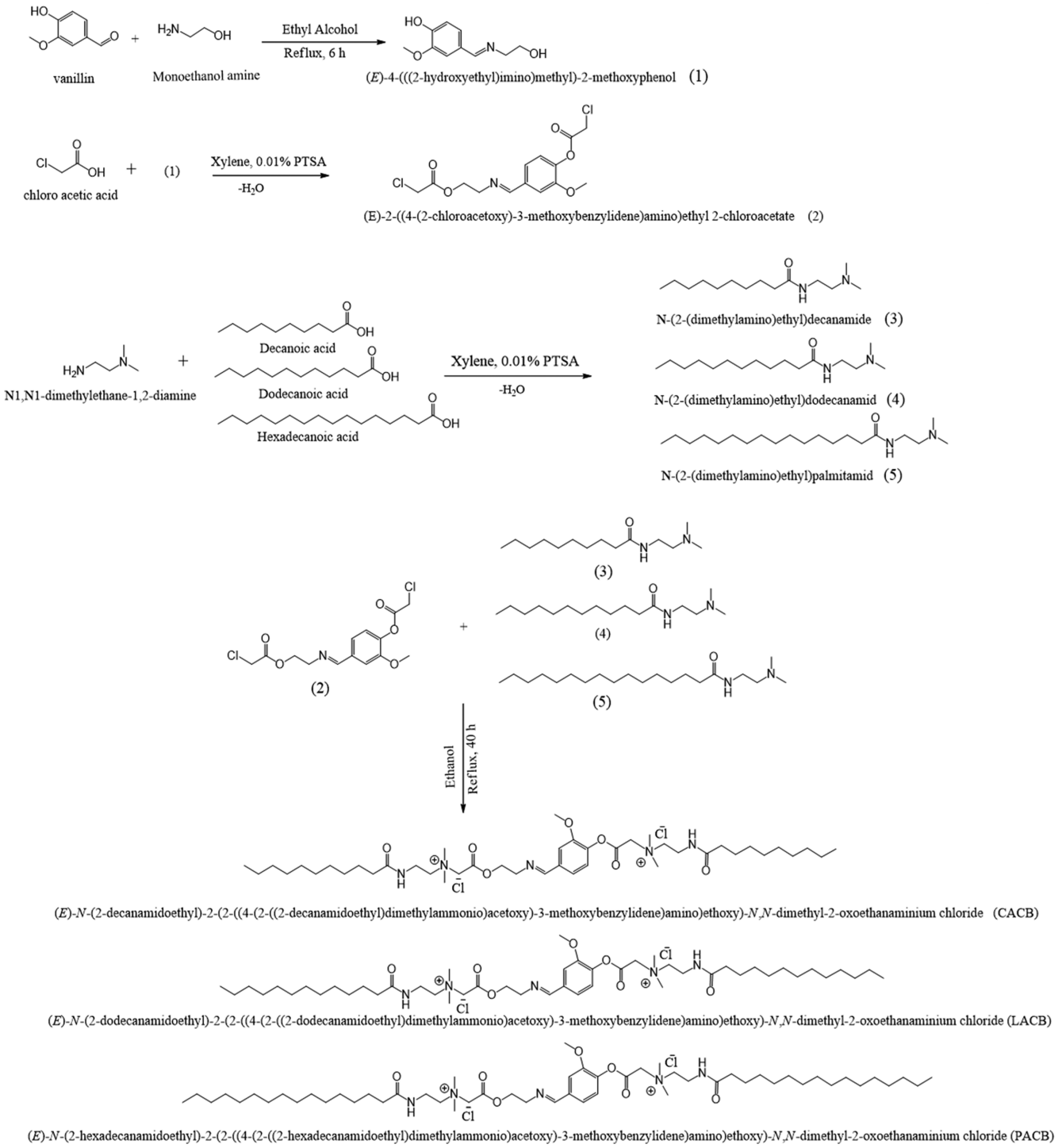
All chemicals involved in the synthesis process of Gemini surfactants were used as received without any further purification. Decanoic (≥99%), dodecanoic (≥99%), and hexadecanoic acids (≥98%) were purchased from Merck (Germany). Chloroacetic acid (≥99%), 2-(dimethylamino)ethylamine (≥98%), and silver nitrate ($AgNO_3$) (≥99%) were purchased from Sigma Aldrich (USA). Both vanillin (≥99%) and monoethanolamine (≥99%) were supplied by Acros (USA). All the solutions were prepared using Milli-Q water (doubly distilled-deionized water with specific conductivity 1-2 μS cm^{-1}).

2. Synthesis Procedures

2-1. Multi-carbonyl Gemini Cationic Surfactant Preparation

The chemical reactions for the target Gemini cationic surfactant are outlined in Scheme 1. For simplicity, they are called CACB,

†To whom correspondence should be addressed.
E-mail: Dhkim1@skku.edu
Copyright by The Korean Institute of Chemical Engineers.



Scheme 1. Reaction pathway of the multi-carbonyl Gemini cationic surfactants, CACB, LACB and PACB.

LACB & PACB, as demonstrated in Scheme 1.

2-1-1. Synthesis of Dichloroester of Vanillin Schiff Base

Monoethanolamine (4.02 g) was refluxed with a stoichiometric amount of vanillin (10 g) in 100 mL of absolute ethanol for 6 h to obtain the corresponding azomethine (Compound 1 with yield percent 89%, Scheme 1) after solvent evaporation and sample purification. The obtained Schiff base 1 was esterified with chloroacetic acid, where 0.02 mole of compound 1 (3.9 g) was refluxed using a Dean-Stark apparatus with 0.04 mole of chloroacetic acid (3.8 g) in the presence of 150 mL of xylene and the catalyst *p*-toluenesulfonic acid (0.01%) [26]. The reaction was complete as a predetermined amount of released water was separated in the bottom of the Dean-Stark tube (0.7 mL). The reaction mixture was then dried in an oven, and the obtained solid materials were crystallized using diethyl ether to remove the catalyst and obtain the dichloroester of the Schiff base (Compound 2 with a yield percent of 78%), as de-

scribed in Scheme 1.

2-1-2. Preparation of Fatty Amides

Three different fatty amides were prepared as described in Scheme 1, where 0.02 moles of 2-(dimethylamino)ethylamine (1.77 g) was refluxed with stoichiometric amounts of capric acid (3.45 g), lauric acid (4 g), and palmitic acid (5.13 g) separately in a Dean-Stark apparatus with 150 mL xylene and 0.01% *p*-toluenesulfonic acid [27]. The reaction was complete as a predetermined amount of released water (0.36 mL) accumulated in the bottom of the Dean-Stark tube. The products obtained after recrystallization and purification were labeled 3, 4, and 5 with a yield percent of 82, 80 and 79%, respectively, as shown in Scheme 1.

2-1-3. Preparation of the Desired Multi-carbonyl Gemini Surfactant

Next, 0.02 mole of the prepared dichloroester of the vanillin Schiff base (2) was refluxed separately for 40 h with 0.04 mole of individually prepared fatty amides 3, 4, and 5 in ethyl alcohol. Finally the reaction mixture was dried in an oven at 85 °C overnight. The obtained solid materials were crystallized using diethyl ether. The three obtained multi-carbonyl Gemini surfactants were (E)-N-(2-decanamidoethyl)-2-(2-((4-(2-((2-decanamidoethyl)dimethylammonio)acetoxy)-3-methoxybenzylidene)amino)ethoxy)-N,N-dimethyl-2-oxoethanaminium chloride (CACB) (with a yield percent of 77%), (E)-N-(2-dodecanamidoethyl)-2-(2-((4-(2-((2-dodecanamidoethyl) dimethylammonio)acetoxy)-3-methoxybenzylidene)amino)ethoxy)-N,N-dimethyl-2-oxoethanaminium chloride (LACB) with a yield percent of 74%, and (E)-N-(2-hexadecanamidoethyl)-2-(2-((4-(2-((2-hexadecanamidoethyl)dimethylammonio)acetoxy)-3-methoxybenzylidene)amino)ethoxy)-N,N-dimethyl-2-oxoethanaminium chloride (PACB) with a yield percent of 76%, which contained 10, 12, and 16 carbon atoms in their tails, respectively.

2-2. Preparation of AgNPs

A photochemical reduction method was used for preparing AgNPs where the sunlight can initiate the reduction process in existence of the synthesized amphiphilic multi-carbonyl Gemini, as a capping agent as well as accelerator for the $AgNO_3$ reduction. In the method, 10 mL of a 2 mM silver nitrate aqueous solution was mixed with 10 mL of 2 mM CACB, LACB or PACB aqueous solution. Each mixture was exposed to sunlight for 5 min, where rapid changes in solution color were observed, indicating the formation of AgNP colloids [28].

3. Structure Characterization

The chemical structures of laboratory prepared multi-electronic rich CACB, LACB and PACB and amphiphilic properties of the AgNPs were investigated by Fourier-transform infrared spectroscopy (FTIR), UV-Vis spectroscopy, transmission electron microscopy (TEM), dynamic light scattering (DLS) as well as proton nuclear magnetic resonance spectroscopy (^{1}H NMR). The instruments are described in the Supporting Information (section 1).

4. Surface Tension (γ)

The surface parameters of CACB, LACB and PACB in their aqueous solution were studied at 20, 40, and 60 °C with temperature uncertainty ±0.1 °C. Their corresponding CMCs were determined by measuring solution surface tension (γ) using a tensiometer-K6 device (Krüss Company, Germany) based on ring method measurements with uncertainty ±0.2 mN/m. Every concentration was maintained for 30 min to establish equilibrium before measurement. Each experiment was repeated triplicate with 5 min between each measurements, and the average was calculated and used for further study [29]. The specified CMCs of the CACB, LACB and PACB aqueous solutions at 20, 40, and 60 °C corresponded to the inflection points in γ versus [log C] plots with uncertainty ±(0.05-0.1) mM.

The maximum saturation by the synthesized amphiphilic expressed as maximum surface excess (Γ_{max}), which is the CACB, LACB or PACB amphipathic compound concentration at the solution interface per unit area. This was computed utilizing Eq. (1) (Gibbs adsorption equation) [4]:

$$\Gamma_{max} = -\left(\frac{1}{2.303 n R T}\right)\left(\frac{\delta\gamma}{\delta \log c}\right)_T \quad (1)$$

where n=3 in case of monovalent counterions connected with Gemini cationic surfactants, R refer to the gas constant whereas both T and ($\delta\gamma/\delta$ log c) point to absolute temperature and surface pressure, respectively.

The minimum surface area (A_{min}) of CACB, LACB & PACB was computed based on Gibbs adsorption equation (Eq. (2)), describing the average area occupied by the synthesized multi-electronic rich gemini unimer (in A^2) at the solution interface [30], where N is Avogadro's number.

$$A_{min} = \frac{10^{16}}{\Gamma_{max} N} \quad (2)$$

The effectiveness of CACB, LACB or PACB (π_{CMC}) corresponds to the difference in γ values of distilled water at surface (γ_o) in absence of prepared amphiphilic compound and that correspond to the CMC (γ_{CMC}), as expressed in Eq. (3):

$$\pi_{CMC} = \gamma_o - \gamma_{CMC} \quad (3)$$

The efficiency C_{20} of the synthesized multi-electronic rich Gemini surfactant CACB, LACB or PACB corresponds to their concentration, which has the tendency to induce reduction in the γ by 20 mN/m.

5. Specific Electrical Conductivity

The specific electrical conductance of prepared CACB, LACB and PACB aqueous solutions at 20, 40, and 60 °C was used for determining CMCs. The specific electrical conductivity was performed using a Cond-3210 SET Tetra-Con 325 (1 Probe) device. The degree of counterion dissociation (α) of CACB, LACB and PACB was determined according to Frahm's method [31]. The critical micelle concentration we measured based on the inflection point in the specific conductivity-concentration with uncertainty ±(0.08-0.16 mM). The uncertainty of the measured conductivity is ±0.5 μS cm^{-1}.

6. Emulsion Stability and Foam Power

The emulsion stability of CACB, LACB and PACB was appraised by vigorously shaking 10 mL of a 0.1% of each prepared multi-electronic rich Gemini amphiphilic aqueous solution and 10 mL non-polar phase (light paraffin oil) at room temperature (25 °C) utilizing a 50 mL measuring cylinder with stopper. The stabilities of CACB, LACB and PACB emulsion were obtained by estimating the duration required for separating 9 mL of pure aqueous phase from the emulsified mixture with uncertainty ±0.5 minute [32].

The foam powers were determined by vigorously shaking 100 mL of CACB, LACB & PACB (0.1%) amphiphilic aqueous solution in a 250 mL stoppered cylinder for 5 minutes. Then the foam power was acquired by the height of the initiated foam with uncertainty ±2 mL, while its stability was indicated by time required to reach half of the initially produced foam height with uncertainty ±0.3 minute [33].

7. Biological Activity

The biocidal performance of the synthesized CACB, LACB and PACB and their AgNP colloids against some pathogenic species of bacteria and fungi was appraised utilizing the modified agar diffusion method [34] at Micro Analytical Lab (Cairo University, Egypt). The experimental details were provided in a previously published work [33]. The antibacterial activity was examined for *Candida albicans*, *Aspergillus flavus*, *Pseudomonas aeuroginosa* (G−), *Escherichia coli* (G−), *Bacillus pumilus* (G+), *Staphylococcus aureus* (G+). The inhibition zone diameter (mm) refers to the corresponding antibacterial activity with uncertainty ±0.5 mm.

The antibiotic effect against SRB was conducted utilizing a serial dilution method [35]. The contaminated water by SRB was obtained by Petrobel Petroleum Company (Egypt) and subject to growth to reach 10^9 bacteria cells/ml. Three doses (1, 0.5, and 1 mM) of the CACB, LACB and PACB and colloidal AgNPs were tested against 3.0 h as incubation contact time with uncertainty ±10 Cell/mL.

RESULTS AND DISCUSSION

1. Structure Confirmation

The reaction pathway of the newly prepared multi-electronic rich Gemini amphiphiles was monitored with FTIR and ^{1}H NMR

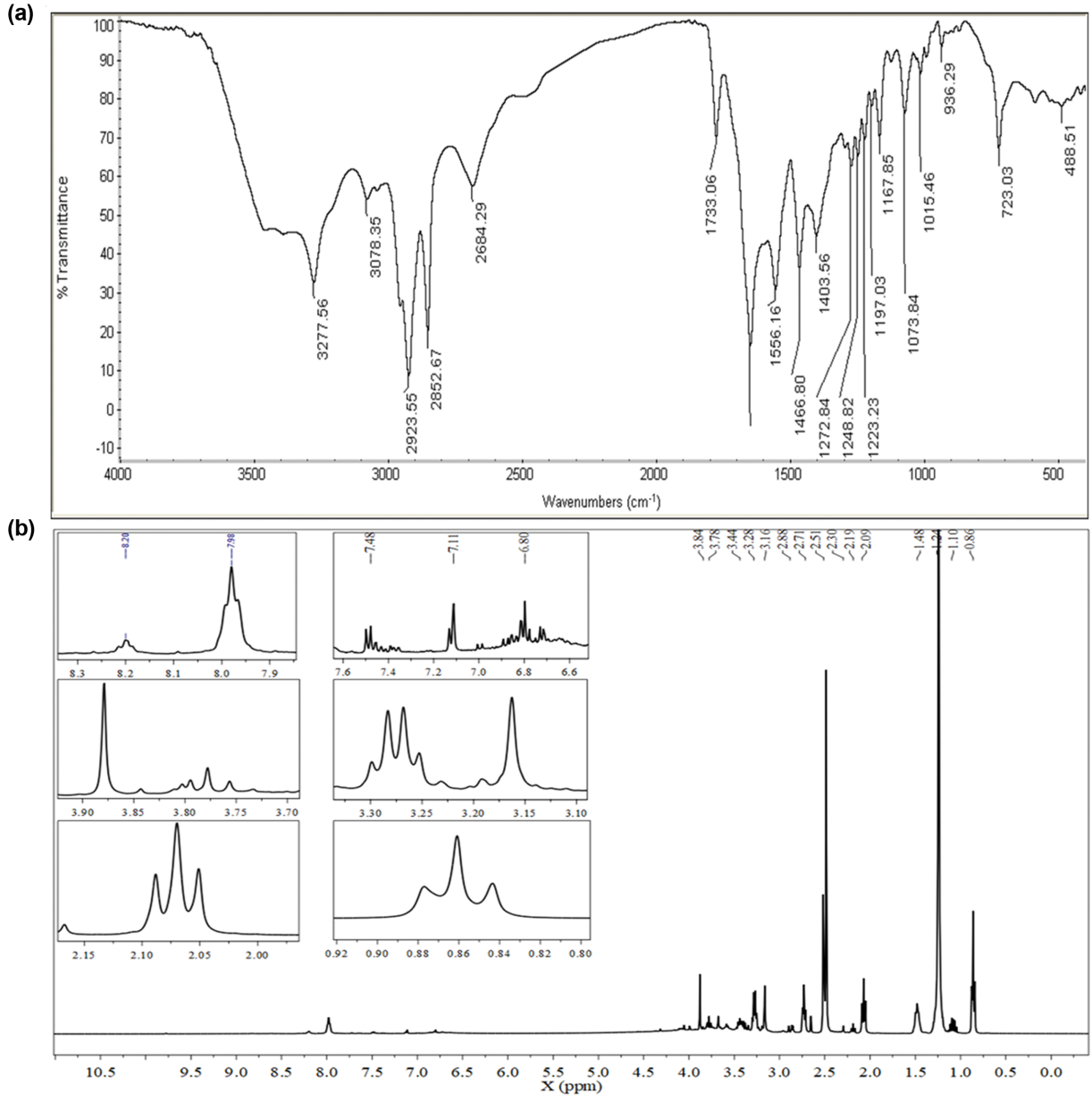


Fig. 1. (a) FTIR and (b) ^{1}HNMR spectrum of freshly prepared Gemini cationic amphiphilic LACB.

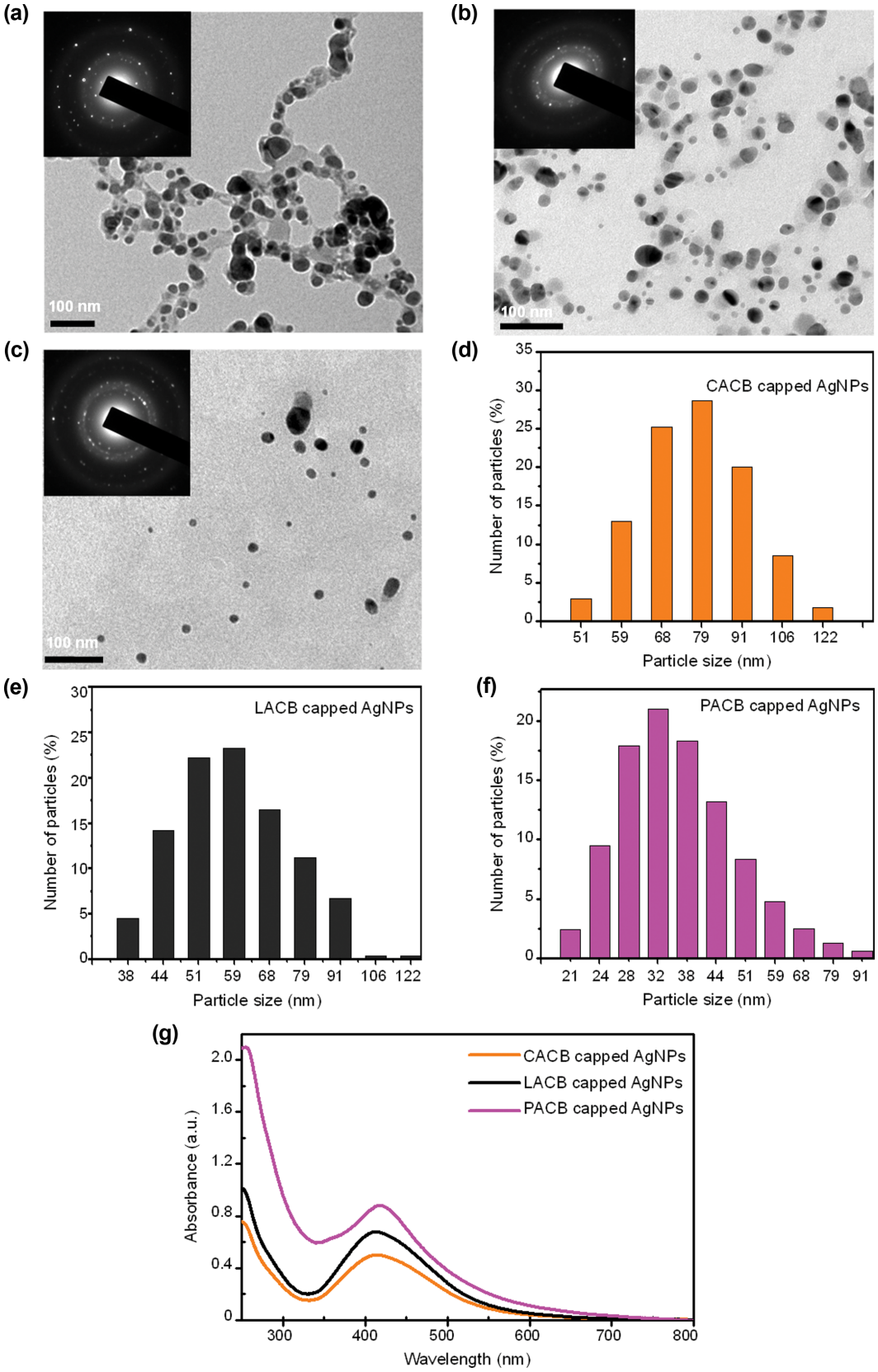


Fig. 2. (a)-(g) AgNPs characterization: (a)-(c) TEM images of synthesized AgNPs capped with synthesized Gemini cationic amphiphilic CACB, LACB & PACB, respectively (insets are the corresponding selected area electron diffraction pattern). (d)-(f) Size distributions of AgNPs capped with CACB, LACB and PACB, respectively. (g) UV-Vis spectra of AgNPs capped with CACB, LACB and PACB, respectively.

spectroscopy. Fig. 1(a) provides the FTIR spectra of LACB, confirming the main characteristic functional groups in the multi-carbonyl Gemini surfactant. The bands at 1,733, 1,670, and 1,556 cm^{-1} correspond to ester carbonyl, amide carbonyl, and C=N- groups, respectively, while the amino groups appeared at 3,277.56 cm^{-1}. The other bands at 1,073, 1,176, 1,381, 1,403, 1,466, 2,923, 2,852.67 and 3,078.35 cm^{-1} represent ether C-O, C-N, CH_3 bending, CH_2 bending, C=C, asymmetric and symmetric aliphatic -C-H & aromatic CH groups, respectively.

Fig. 1(b) shows the ^{1}H NMR spectra of the LACB surfactant. δ 0.86 (t, 6H, 2CH_3 alkyl chain), 1.1-1.24 (m, 32H, 2 (HNCO-$CH_2CH_2(CH_2)_8CH_3$)), 1.48 (m, 4H, 2 (HNCOCH_2CH_2(CH_2)$_8$CH_3)), 2.09 (m, 4H, 2 (HNCOCH_2CH_2(CH_2)$_8$CH_3)), 2.19 (t, 2H, PhOC-$OCH_2(CH_3)_2N^+CH_2CH_2NH$), 2.3 (t, 2H, $PhOCOCH_2(CH_3)_2N^+$ CH_2CH_2NH), 2.51 (s, 12H, $PhOCOCH_2(CH_3)_2N^+CH_2CH_2NH$), 2.7 (t, 2H, $CH=NCH_2CH_2OCOCH_2(CH_3)_2N^+CH_2CH_2NH$), 2.88 (t, 2H, $CH=NCH_2CH_2OCOCH_2(CH_3)_2N^+CH_2CH_2NH$), 3.16 (s, 3H, PhOC$H_3$ methoxy group), 3.28 (t, 2H, $CH=NCH_2CH_2OCO$-$CH_2(CH_3)_2N^+$), 3.44 (t, 2H, $CH=NCH_2CH_2OCOCH_2(CH_3)_2N^+$), 3.7 (s, 2H, $CH=NCH_2CH_2OCOCH_2(CH_3)_2N^+$), 3.77 (t, 2H, t, 2H, $HOCH_2CH_2OCH_2CH_2N^+$), 3.84 (s, 2H, $PhOCOCH_2(CH_3)_2N^+$ CH_2CH_2NH) 6.8-7.48 (s, 3H, aromatic protons), 7.9 (t, 2H, 2 (H$NCOCH_2CH_2(CH_2)_8CH_3$)), 8.2 (s, 1H, CH=NCH_2CH_2OCO-$CH_2(CH_3)_2N^+$).

2. Silver Nanoparticle Characterization

The AgNPs were prepared by photo-reduction reaction using sunlight as reducing agent. The light induced radiolysis of water generating hydrogen, hydrogen peroxide, hydrogen radical, hydroxyl radical as well as solvated electron. Each solvated electron, $H^{\cdot}$ atom and H_2O_2 can act as a reducing agents for Ag^+ into Ag atom; however, their concentration (from radiolysis process) is insufficient to induce Ag^+ reduction effectively. The synthesized surfactants have the ability to scavenge the hydrogen radical, hydroxyl radical (from radiolysis process), which triggers more solvated electrons production, consequently the reduction efficiency increases [19].

The roles of CACB, LACB and PACB in the preparation of AgNPs and their effects on the formed nanoparticles structure were assessed by TEM, DLS and UV-Vis spectroscopy. The morphology of the obtained AgNPs using CACB, LACB and PACB as capping agents is illustrated in Figs. 2(a)-(c). CACB, LACB and PACB produced spherical AgNPs, but there was a clear difference between the preparations in terms of the aggregation of obtained AgNPs. As shown in Figs. 2(a)-(c), the aggregation of the as-prepared AgNPs decreased with increasing the length synthesized multi-electronic rich Gemini surfactant tail. There was decreasing AgNP aggregation with elongation of the surfactant tail because of increasing adsorption tendency with a longer hydrocarbon chain (PACB).

The crystallinity of each of the prepared AgNPs capped by the CACB, LACB and PACB is indicated by the selected area electron diffraction (SAED) patterns in Figs. 2(a)-(c) (inset images). PACB provided more crystalline AgNPs, while CACB produced fewer crystalline AgNPs.

CACB, LACB and PACB produced AgNPs with size distributions of 65±18, 50±14 and 32±10 nm, respectively (Figs. 2(d)-(f)), showing that an increased hydrocarbon chain length of the synthesized amphiphilic compounds induced AgNPs with narrower size distribution with a smaller particle size. The zeta potential of the prepared AgNPs was 13.5±3.3, 39.5±11.5, and 51±8 mV with CACB, LACB and PACB, respectively. The positive zeta potential revealed the presence of layer from the synthesized multi-electronic Gemini cationic amphiphilic that have positive charge around the produced AgNPs. A high zeta potential is correlated to the high stability of the produced AgNPs in the solution, where values larger than +30 mV indicated preparation of a stable nanocolloid [36,37]. Clearly, using PACB (with a long hydrocarbon chain) produced more stable AgNPs colloids compared to CACB (with a shorter hydrocarbon chain), which produced less stable colloids and resulted in more aggregation, as shown in Figs. 2(a)-(c). The longer hydrocarbon chain length also showed a higher adsorption tendency at the interfaces, consequently forming a better protective layer around the produced AgNPs and thereby preventing aggregation and improving stability [25,38-40]. The long hydrophobic chain of the Gemini surfactant tends to induce dispersion of synthesized AgNPs coming from the increase of the repulsion between the hydrophobic tails around AgNPs, hence a sharp absorption peak is obtained. Whereas, short hydrophobic chain of the Gemini surfactant appears to induce more aggregation of AgNPs due to less repulsion, hence a broad absorption peak is obtained [23].

Fig. 2(g) compares the absorption spectra of the synthesized AgNPs capped with Gemini CACB, LACB and PACB, showing a band at wavelength λ of 420 nm characteristic for AgNPs surface

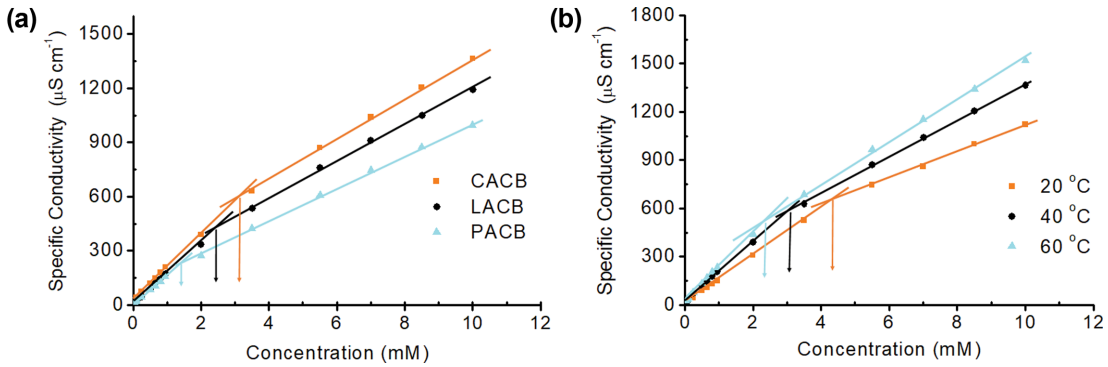


Fig. 3. (a) Plots describing specific electrical conductivity-concentrations of CACB, LACB and PACB aqueous solutions at 40 °C. (b) Plots describing specific electrical conductivity-concentrations of CACB at 20, 40, and 60 °C.

Table 1. Surface parameters of the prepared multi-electronic rich Gemini amphiphiles (CACB, LACB and PACB) at different temperatures

Property	CACB			LACB			PACB		
	20 °C	40 °C	60 °C	20 °C	40 °C	60 °C	20 °C	40 °C	60 °C
CMC[a], mM	4.45	3.07	2.03	3.07	2.03	1.20	1.54	1.03	0.77
CMC[b], mM	4.53	3.12	2.3	3.12	2.35	1.36	1.68	1.26	0.84
α	0.59	0.60	0.61	0.57	0.59	0.60	0.56	0.57	0.58
C_{20} *10^{-5}, M	5.41	3.31	2.54	1.55	0.74	0.61	0.55	0.31	0.22
π_{CMC}, mN m^{-1}	41.5	40.1	37.4	43.5	42.4	39.4	44.9	43.6	40.2
Γ_{max} *10^{-10}, mol·cm^{-2}	0.62	0.5	0.47	0.64	0.51	0.47	0.67	0.52	0.48
A_{min}, A^2	269.1	331.2	356.8	257.5	325.9	352.3	247.1	319.7	347.4
CMC/C_{20}	82.3	92.6	79.7	198.5	275.4	196.5	277.6	331.1	346.9

plasmon resonance [41]. The absorption intensity of the AgNPs shows an increasing trend with an elongation the surfactant's hydrocarbon tail of the CACB, LACB and PACB, which is directly related to an increased amount of produced AgNPs with increased hydrophobicity [42]. The use of a surfactant with a longer hydrocarbon chain achieved a higher yield with more stability compared to the use of an amphiphilic one with hydrocarbon chain containing fewer carbon atoms.

3. Critical Micelle Concentration (CMC)

The CMCs values of the as-prepared multi-electronic rich Gemini cationic amphiphilic in an aqueous environments were assessed at 20, 40 & 60 °C using specific conductivity and γ measurements. The surfactants had a large effect on solution conductivity. The experimental results showed an inverse relationship between specific electrical conductivity and the length of the synthesized CACB, LACB and PACB hydrocarbon tail, as Fig. 3(a) and Supporting Information Figs. S1 and S2 outline. Furthermore, there was a direct relationship between solution temperature and surfactant solution specific conductivity, as shown in Fig. 3(b) and Supporting Information Figs. S3 and S4.

The calculated α values for the prepared surfactants at 20, 40 and 60 °C, are illustrated in Table 1. As shown, there was an inverse correlation between length of as-synthesized amphiphilic Gemini hydrocarbon tail and conductivity. At the same time, the depicted experimental α values (Table 1) are directly correlated with surfactant solution specific electrical conductivity and temperature. Hydration environment around the amphiphilic hydrophilic head decreased with increasing hydrocarbon tail length. Consequently, the counterions are strongly bonded to the head of CACB, LACB and PACB, which induces a decrease in specific conductivity [43,44]. As solu-

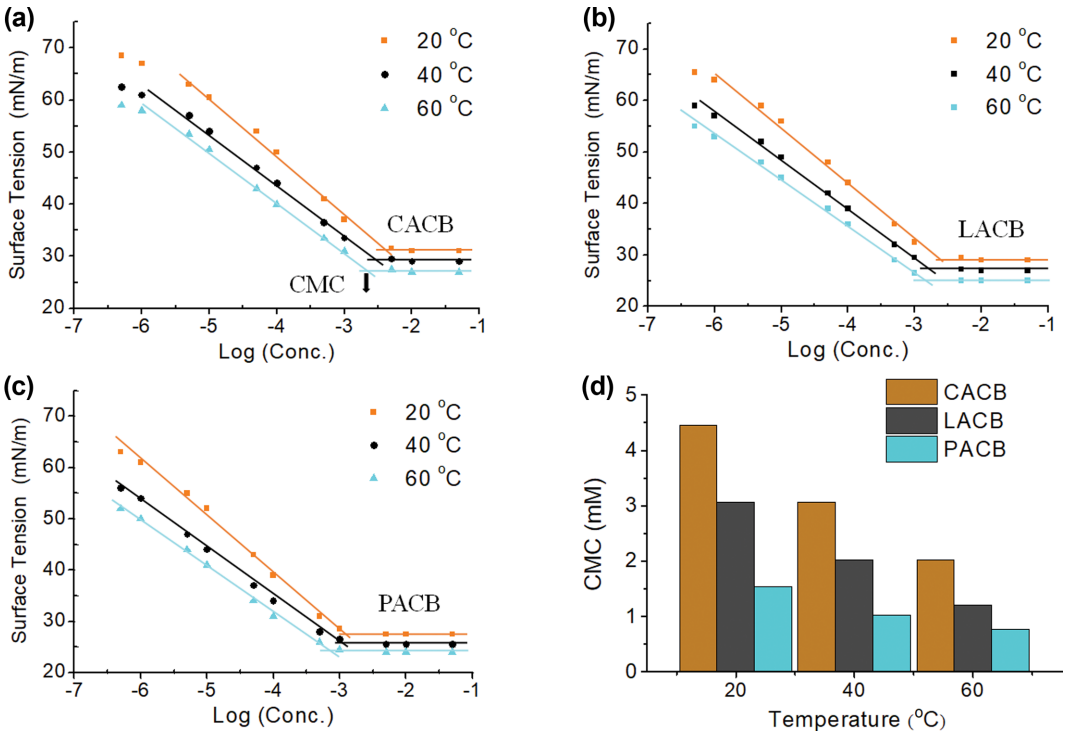


Fig. 4. (a)-(c) The relationship between surface tension-log [C] of prepared CACB, LACB and PACB surfactants, respectively, at various temperatures. (d) Effect of both temperature & hydrocarbon tail length on critical micelle concentration.

tion temperature increased, the bond the amphiphilic counterion and their hydrophilic heads became weaker, and therefore the α values increased [45].

The CMC corresponded to the break-off in electrical conductivity against amphiphilic concentration curve (Figs. 3(a), (b)). At the same time, the CMC values were determined according to γ measurements and corresponded to an abrupt change in the γ-log [C] plot (Figs. 4(a)-(c)). The calculated CMC values of the prepared Gemini amphiphilic CACB, LACB and PACB based on specific conductivity are depicted in Table 1. Figs. 3(a), (b) show a large enhancement in specific conductivity at the CMC, ascribed to an increase in hydration around the head groups in aggregated micelles compared to surfactant unimers. Hydration led to weaker bond strengths between associated counterions, resulting in an increase in specific conductivity. Figs. 4(a)-(c) showed a steady state in γ at a concentration at which micelles start to construct, where the surfactant unimers aggregate in clusters in the solution. Consequently, there was no further reduction in γ.

The experimental values depicted in Table 1 show CMC decreasing with elongation of the hydrocarbon chain of the amphiphilic, as illustrated in Fig. 4(d). Increasing hydrocarbon chain length induces an increase in solution hydrophobic character. Therefore, enhancing the system free energy, which caused the surfactant to either migration and/or micellization inducing decreasing in CACB, LACB and PACB solution energy. Consequently, increasing the surfactant tail length enhanced micelle formation [46,47].

The measured CMC values (Table 1) showed a decrease in CMC at elevated solution temperatures (Fig. 4(d)). Hydration around the hydrophilic head decreased after increasing surfactant solution temperature, which led to increased micellization affinity. At the same time, raising the solution temperature destroyed the water structure that surrounds the tail, which is unfavorable for micellization. The magnitudes of the two aforementioned opposing trends were responsible for the CACB, LACB and PACB surfactant behaviors with temperature. The interpreted experimental data (Table 1) indicate decreasing the CMC with temperature [2,48].

4. Additional Surface Parameters

The maximum concentration of the CACB, LACB and PACB amphiphilic unimers at solution interface and their minimum surface area were computed according to Eqs. (1) and (2), and the data are provided in Table 1, suggesting that the variation of hydrocarbon chain length as well as temperature greatly influence both Γ_{max} and $\mathbf{A}_{min}$. The Γ_{max} of the prepared aqueous solutions of CACB, LACB and PACB increased with increasing amphiphilic hydrophobic character as emphasized in elongation length of double tail involved in the synthesized amphiphilic multi-electronic Gemini CACB, LACB and PACB (Table 1).

The $\mathbf{A}_{min}$ of the prepared Gemini amphipathic CACB, LACB and PACB decreased as carbon atoms involved in the two hydrocarbon tails increased. Increasing solution hydrophobicity promoted migration of surfactant unimers, where they were adsorbed at the aqueous interface. Therefore, a dense layer was expected to form. The dense packing forced the surfactant unimers to orient vertically at the solution interface. Consequently, $\mathbf{A}_{min}$ decreased as increasing amphiphilic hydrophobic character as emphasized in elongation length of double tail involved in the synthesized amphiphilic multi-electronic Gemini CACB, LACB and PACB [49-51].

Table 1 outlines the effects of solution temperature on Γ_{max} and $\mathbf{A}_{min}$, where $\mathbf{A}_{min}$ increased and Γ_{max} decreased as the solution temperature raised up to 60 °C. As the solution temperature increased, the activation energies of CACB, LACB and PACB unimers also increased, which increased the repulsion induced between the double hydrophobic tails and the aqueous medium. Overall, this forced the unimers to orient more horizontally at the phase interface, leading to an increase in $\mathbf{A}_{min}$. An increased occupied area of the surfactant with temperature promote a decrease in the amount of accumulated CACB, LACB or PACB unimers at the solution interface, such that Γ_{max} decreased [52,53].

The experimental effectiveness π_{CMC} of the surfactants at temperatures of 20, 40, and 60 °C, as shown in Table 1, indicate that PACB was the most effective for γ reduction. The π_{CMC} values of the CACB, LACB and PACB at 45 °C were 40.1, 42.4, and 43.6 mN m^{-1}, respectively (Table 1). As reported previously, the most effective surfactant is one exhibiting the highest CMC/C_{20} value [54,55].

The C_{20} values for CACB LACB and PACB increased with increasing solution temperature as well as with increasing carbon atoms number in doubly tailed, as shown in Table 1. A more extensive reduction in γ is predicted for an increased hydrophobic character as emphasized in elongation length of double tail involved in the synthesized amphiphilic multi-electronic Gemini CACB, LACB and PACB, hence an increasing affinity for amphiphilic unimers migration to the phase interface (Supporting Information Figs. S5-S7) [56]. Raising the temperature resulted in dispatching the water molecules surrounding the head of the synthesized CACB LACB and PACB (the system hydrophobicity increased), which led to additional migration to the interface and a greater influence on γ [3].

5. Thermodynamic View of Surfactant Behavior

The thermodynamic behaviors of CACB, LACB and PACB in the aqueous phase were outlined based on Gibbs standard equations (Eqs. (4)-(9)) at 20, 40 and 60 °C. The computed thermodynamics were the standard free energy of micellization (ΔG^o_{mic}) and adsorption (ΔG^o_{ads}), changes in micellization entropy (ΔS_{mic}) and adsorption entropy (ΔS_{ads}), and changes in micellization enthalpy (ΔH_{mic}) and adsorption enthalpy (ΔH_{ads}).

$$\Delta G^o_{mic} = 2(1.5-\alpha)RT\ \ln(X_{CMC}) \tag{4}$$

$$\Delta G^o_{ads} = \Delta G^o_{mic} - 6.023\times10^{-2}(\pi_{CMC}/\Gamma_{Max}) \tag{5}$$

$$\Delta H_{mic} = -T^2\left(\frac{\partial\left(\frac{\Delta G^o_{mic}}{T}\right)}{\partial T}\right)_p \tag{6}$$

$$\Delta H_{ads} = -T^2\left(\frac{\partial\left(\frac{\Delta G^o_{ads}}{T}\right)}{\partial T}\right)_p \tag{7}$$

$$\Delta S_{mic} = \frac{\Delta H_{mic} - \Delta G^o_{mic}}{T} \tag{8}$$

$$\Delta S_{ads} = \frac{\Delta H_{ads} - \Delta G^o_{ads}}{T} \tag{9}$$

Table 2. Thermodynamic insights of micellization and adsorption processes of the amphiphilic CACB, LACB and PACB

Surfactant	Temp. °C	ΔG^{o}_{mic} kJ mol^{-1}	ΔH_{mic} kJ mol^{-1}	ΔS_{mic} J mol^{-1} K^{-1}	ΔG^{o}_{ads} kJ·mol^{-1}	ΔH_{ads} kJ·mol^{-1}	ΔS_{ads} kJ·mol^{-1} K^{-1}
CACB	20	−41.83	16.12	197.64	−48.54	18.66	229.21
	40	−45.81	18.40	204.99	−53.80	21.30	239.78
	60	−50.03	20.82	212.64	−58.06	24.10	246.58
LACB	20	−44.22	17.77	211.41	−50.97	22.26	249.74
	40	−48.11	20.27	218.34	−56.44	25.40	261.30
	60	−53.01	22.95	227.95	−61.37	28.75	270.46
PACB	20	−47.62	15.30	214.62	−54.30	20.62	255.54
	40	−52.54	17.46	223.50	−60.94	23.53	269.70
	60	−56.49	19.76	228.86	−64.91	26.63	274.73

Uncertainty of ΔG^{o}_{mic}, ΔH_{mic} and ΔS_{mic} calculation was ±0.8%, while ΔG^{o}_{ads}, ΔH_{ads} and ΔS_{ads} was 0.9%.

Table 3. Emulsion, foam and interfacial performance of the prepared Gemini cationic amphiphilic at 25 °C

Surfactant	Emulsion stability (h)	Interfacial tension (mN/m)	Foam height (mL)	Foam stability (h)
CACB	1	7	130	1
LACB	1.2	5	200	2.5
PACB	7	4	180	3.5

X_{CMC} is the CMC molar fraction. The obtained thermodynamic parameters (Table 2) predict a higher affinity of CACB, LACB and PACB amphiphilic unimers to adsorption process compared to their affinity to aggregate in micelles structures, as shown in Table 2. The change in ΔG^{o}_{ads} of CACB, LACB and PACB in the aqueous phase at all of the tested temperatures was higher than the corresponding ΔG^{o}_{mic}, which shows their highest adsorption tendency at the aqueous phase interface until saturation, after which they aggregated in the solution in micelles [57-59]. The thermodynamic calculations also demonstrated that the adsorption trend at the solution phase interface as well as micellization in the solution bulk were temperature and hydrophobicity dependent. The negative value of ΔG^{o}_{ads} and ΔG^{o}_{mic} increased in accordance with the carbon atoms number in the double hydrocarbon tail increased, as shown in Table 2.

The increased solution hydrophobicity as a result of the increasing amphiphilic hydrophobic character as emphasized in elongation length of double tail involved in the synthesized amphiphilic multi-electronic Gemini CACB, LACB and PACB, led to decreasing the affinity of the surfactants for the aqueous phase and more destroying the homogenous structure of water. Therefore, enhancing system free energy, inducing the amphiphilic CACB, LACB and PACB unimers migration to the aqueous phase interface and/or aggregate in clusters to minimize the solution free energy. The thermodynamic calculations predicted an increase in adsorption and micellization affinity at elevated solution temperatures. In Table 2, the negative values of both ΔG^{o}_{mic} and ΔG^{o}_{ads} increased as the solution temperature increased. Water hydration around the amphiphilic hydrophilic decreased with increasing amphiphilic solution temperature, which led to an increase in system free energy, promoting the amphiphilic unimer aggregation in micelles and/or migration to the solution interface [60].

6. Emulsification Power, Interfacial Tension, and Foam Power

CACB, LACB and PACB showed high stability for the emulsion induced between light paraffin oil and aqueous phase at 25 °C, as shown in Table 3. The stability of an emulsion of the surfactant with light paraffin oil increased as the surfactant's hydrocarbon tail became longer. The emulsion stability of aqueous solutions of CACB, LACB and PACB with paraffin oil at 25 °C was 1, 1.2, and 7 h, respectively. The high emulsion stability obtained by LACB with a longer hydrocarbon tail suggests its use as an emulsifier in applications such as paints, pharmaceuticals, and water-soluble corrosion inhibitors [61].

CACB, LACB and PACB showed a high affinity to reduce interfacial tension between the non-polar light paraffin oil and water at 25 °C to 7, 5, and 4 mN/m, respectively (Table 3), which emphasized the higher migration affinity to the interface. Elongation the double hydrophobic tail of the synthesized CACB, LACB and PACB led to a decrease in interfacial tension. PACB may be used to enhance oil recovery because of its lower interfacial tension [62]. LACB had a higher foam power, where its foam height at 25 °C was 200 mL, while PACB had a higher emulsion stability, as shown in Table 3.

7. Antibacterial and Antifungal Activities

The activities of CACB, LACB PACB and their AgNP colloids toward common bacteria and fungi were appraised using filter paper disc agar method. The provided results (Table 4) indicate a relationship between the amphiphilic chemical structure of each surfactant and their performance as an antimicrobial agent. The antibiotic efficiency increased with the elongation of the double hydrocarbon tail to a definite chain length and then decreased (Table 4). This phenomenon, referred to as a "cut-off effect", mainly depends on the magnitude of the surfactant surface activity (such as CMC, maximum surface excess, and adsorption free energy), which in turn depends on the surfactant chemical structure [63-67]. The CMC decreased as the double hydrocarbon chain length elongated, indicating that a lower concentration of surfactant can reach the cell membrane of the bacteria; thus, a decrease in the activity was

Table 4. The antibiotic effects of prepared CACB, LACB & PACB and their AgNPs against some of bacteria and fungi

Organism / Compound	Inhibition zone diameter (mm/mg sample)					
	Pseudomonas aeuroginosa	*Escherichia coli*	*Bacillus pumilus*	*Staphylococcus aureus*	*Candida albicans*	*Aspergillus flavus*
CACB	12	11	12	9	9	9
LACB	15	16	15	13	13	15
PACB	14	14	13	12	10	8
CACB-AgNPs	14	15	13	13	10	12
LACB-AgNPs	19	21	17	16	12	12
PACB-AgNPs	17	18	15	15	12	9

Table 5. Biological activity of prepared CACB, LACB and PACB surfactants against SRB bacteria obtained using a serial dilution method

Conc., mM / Compound	0.1	0.5	1
	Bacteria count (Cells/mL)		
Blank		10^9	
CACB	10^4	10^3	10^2
LACB	10^3	10^2	Nil
PACB	10^3	10^2	10
CACB-AgNPs	10^3	10^2	Nil
LACB-AgNPs	10^2	Nil	Nil
PACB-AgNPs	10^3	10	Nil

anticipated. As described in Section 3.5, the adsorption affinity toward the surface increased with increasing surfactant tail length, so the antibacterial effect was predicted to increase. Finally, the net magnitudes of all of the surface parameters were responsible for the activity of the designated surfactant toward the microorganism. The experimental results showed that the synthesized surfactant LACB was the most effective. The experimental data in Table 4 indicate the enhanced effect of the synthesized amphiphilic compounds on the AgNPs, where the AgNP colloids with CACB, LACB and PACB had an increased antibacterial effect as a result of AgNP accumulation and interactions on the cell membrane. With AgNPs penetration through the cytoplasmic cell wall membrane (in addition to the surfactant with its counter ion) destroyed the selective permeability, causing cell death.

The activities of CACB, LACB and PACB and their colloid phases with the AgNPs were assessed against SRB using a serial dilution method. As shown in Table 5, the prepared antibiotic compounds had an effective killing action against SRB. The results indicated that the hydrocarbon tail had an influence on the activity against SRB. As shown, the activity enhanced as the length of the double hydrocarbon tail become longer from 10 to 12 carbon atoms and then decreased at 16 carbon atoms. LACB and its nanocolloid with AgNPs had the strongest antibiotic effects against SRB.

The killing mechanism depended on the ability of the prepared Gemini surfactant to adsorb on the cytoplasmic bacteria cell wall membrane, which was mainly characterized by its hydrophobic nature. The presence of some electronic rich functional groups, such as oxygen, double bonds, carbonyl groups, as well as nitrogen (in addition to positive charge), enhanced the binding to the membrane. With the adsorption of synthesized amphiphilic at the cell wall membrane, the counter ions and hydrocarbon tail penetrated the cytoplasmic cell and causing cell death throughout destroying the selective permeability regarding to cell wall [68].

CONCLUSION

Three multi-carbonyl Gemini surfactants with different hydrophobic tail, CACB, LACB and PACB were synthesized. FTIR and ^{1}HNMR spectroscopy confirmed the main functional groups and proton distribution of the synthesized surfactant. The tail length of Gemini surfactant was found to affect the stability and size of synthesized AgNPs. The surfactant PACB possessing the longest tail length produced AgNPs with smallest size and higher stability. The hydrocarbon tail lengths also affected the surface activity; the micellization process was enhanced as both the number of carbon atoms in the tail and phase temperature increased. Thermodynamic calculations showed that adsorption of CACB, LACB and PACB at the solution interface was preferred, then their aggregation into micelles. The Gemini surfactants with a 12-carbon chain showed the highest antimicrobial activity to sulfate-reducing bacteria, with a maximum efficiency at a concentration of 1 mM.

ACKNOWLEDGEMENTS

This work was financially supported by a National Research Foundation of Korea (NRF) grant funded by the Ministry of Education, Science and Technology (NRF-2018R1D1A1B07041584).

SUPPORTING INFORMATION

Additional information as noted in the text. This information is available via the Internet at http://www.springer.com/chemistry/journal/11814.

REFERENCES

1. I. Aiad, M. M. El-Sukkary, A. El-Deeb, M. Y. El-Awady and S. M. Shaban, *J. Surfactants Deterg*, **15**, 359 (2012).
2. A. Chatterjee, S. P. Moulik, S. K. Sanyal, B. K. Mishra and P. M. Puri, *J. Phys. Chem. B*, **105**, 12823 (2001).
3. I. Aiad, S. M. Shaban, H. Y. Moustafa and A. Hamed, *Prot. Met.*

Phys. Chem. Surf., **54**, 135 (2018).
4. L. D. Song and M. J. Rosen, *Langmuir*, **12**, 1149 (1996).
5. I. A. Khan, R. Mohammad, M. S. Alam and D. Kabir-Ud, *J. Chem. Eng. Data*, **55**, 370 (2010).
6. M. S. Alam, V. Nareshkumar, N. Vijayakumar, K. Madhavan and A. B. Mandal, *J. Mol. Liq.*, **194**, 206 (2014).
7. I. A. Khan, R. Mohammad, M. S. Alam and D. Kabir-Ud, *J. Surfactants Deterg*, **13**, 179 (2010).
8. M. S. Alam and A. B. Mandal, *J. Mol. Liq.*, **212**, 237 (2015).
9. N. Fatma, M. Panda, D. Kabir-Ud and M. Beg, *J. Mol. Liq.*, **222**, 390 (2016).
10. F. Li, M. J. Rosen and S. B. Sulthana, *Langmuir*, **17**, 1037 (2001).
11. M. S. Alam, A. M. Siddiq, D. Natarajan, M. S. Kiran and G. Baskar, *J. Mol. Liq.*, **273**, 16 (2019).
12. R. Srivastava and M. S. Alam, *Int. J. Biol. Macromol.*, **122**, 72 (2019).
13. R. Zana, *J. Colloid Interface Sci.*, **248**, 203 (2002).
14. A. Pinazo, R. Pons, M. Bustelo, M. A. Manresa, C. Moran, M. Raluy and L. Perez, *J. Mol. Liq.*, **289**, 111156 (2019).
15. M. S. Alam and A. M. Siddiq, *J. Mol. Liq.*, **242**, 1075 (2017).
16. M. S. Alam, N. Kamely, A. M. Siddiq, K. Madhavan, N. Vijayakumar, V. Nareshkumar and A. B. Mandal, *J. Dispersion Sci. Technol.*, **36**, 1029 (2015).
17. Y. A. Krutyakov, A. A. Kudrinskiy, A. Y. Olenin and G. V. J. R. C. R. Lisichkin, *Russ. Chem. Rev.*, **77**, 233 (2008).
18. S. Agnihotri, S. Mukherji and S. Mukherji, *Rsc Adv.*, **4**, 3974 (2014).
19. S. M. Shaban, I. Aiad, M. M. El-Sukkary, E. A. Soliman and M. Y. El-Awady, *J. Ind. Eng. Chem.*, **20**, 4473 (2014).
20. A. M. Siddiq, T. Parandhaman, A. F. Begam, S. K. Das and M. S. Alam, *Enzyme Microb. Technol.*, **95**, 118 (2016).
21. V. K. Shukla, R. S. Yadav, P. Yadav and A. C. Pandey, *J. Hazard. Mater.*, **213-214**, 161 (2012).
22. M. S. Bakshi, F. Possmayer and N. O. Petersen, *J. Phys. Chem. C*, **112**, 8259 (2008).
23. R. Kaur, K. Singh, P. Khullar, A. Gupta, G. K. Ahluwalia and M. S. Bakshi, *Langmuir*, **35**, 14929 (2019).
24. S. M. Shaban, I. Aiad, M. M. El-Sukkary, E. A. Soliman and M. Y. El-Awady, *Chin. Chem. Lett.*, **26**, 1415 (2015).
25. S. M. Shaban and A. A. Abd-Elaal, *Mater. Sci. Eng. C Mater. Biol. Appl.*, **76**, 871 (2017).
26. N. A. Negm, A. F. El Farargy, A. M. Al Sabagh and N. R. Abdelrahman, *J. Surfactants Deterg*, **14**, 505 (2011).
27. S. M. Shaban, *Rsc Adv.*, **6**, 39784 (2016).
28. S. M. Shaban, I. Aiad, M. M. El-Sukkary, E. A. Soliman and M. Y. El-Awady, *Chin. Chem. Lett.*, **28**, 264 (2017).
29. M. A. Migahed, N. A. Negm, M. M. Shaban, T. A. Ali and A. A. Fadda, *J. Surfactants Deterg*, **19**, 119 (2016).
30. B. Gao and M. M. Sharma, *J. Colloid Interface Sci.*, **404**, 80 (2013).
31. O. Kaczerewska, B. Brycki, I. Ribosa, F. Comelles and M. T. Garcia, *J. Ind. Eng. Chem.*, **59**, 141 (2018).
32. A. R. Tehrani-Bagha, *Colloids Surf. A*, **508**, 79 (2016).
33. S. M. Shaban, A. S. Fouda, S. M. Rashwan, H. E. Ibrahim and M. F. El-Bhrawy, *J. Mol. Liq.*, **221**, 224 (2016).
34. C. Perez, *Acta Biol. Med. Exp.*, **15**, 113 (1990).
35. ASTM D4412-84, Standard test methods for sulfate-reducing bacteria in water and water –formed deposits, 2009.
36. J. Hedberg, M. Lundin, T. Lowe, E. Blomberg, S. Wold and I. O. Wallinder, *J. Colloid Interface Sci.*, **369**, 193 (2012).
37. S. M. Shaban, *J. Mol. Liq.*, **216**, 137 (2016).
38. A. A. Abd-Elaal, N. M. Elbasiony, S. M. Shaban and E. G. Zaki, *J. Mol. Liq.*, **249**, 304 (2018).
39. Y. G. Sun, Y. D. Yin, B. T. Mayers, T. Herricks and Y. N. Xia, *Chem. Mater.*, **14**, 4736 (2002).
40. G. A. Bhaduri, R. Little, R. B. Khomane, S. U. Lokhande, B. D. Kulkarni, B. G. Mendis and L. Siller, *J. Photochem. Photobiol. A.*, **258**, 1 (2013).
41. G. Wei, L. Wang, L. L. Sun, Y. H. Song, Y. J. Sun, C. L. Guo, T. Yang and Z. A. Li, *J. Phys. Chem. C*, **111**, 1976 (2007).
42. A. Biswas, O. C. Aktas, U. Schurmann, U. Saeed, V. Zaporojtchenko, F. Faupel and T. Strunskus, *Appl. Phys. Lett.*, **84**, 2655 (2004).
43. L. F. Zhi, Q. X. Li, Y. L. Li and Y. B. Song, *Colloids Surf. A*, **436**, 684 (2013).
44. L. H. Zhuang, K. H. Yu, G. W. Wang and C. Yao, *J. Colloid Interface Sci.*, **408**, 94 (2013).
45. X. Zhong, J. W. Guo, L. J. Feng, X. J. Xu and D. Y. Zhu, *Colloid Surf. A*, **441**, 572 (2014).
46. I. Aiad, M. M. EL-Sukkary, A. El-Deeb, M. Y. El-Awady and S. M. Shaban, *J. Surfactants Deterg*, **16**, 243 (2013).
47. T. Zhang, X. F. Cao, X. C. Wang and C. C. Song, *J. Mol. Liq.*, **230**, 505 (2017).
48. S. M. Shaban, I. Aiad and A. R. Ismail, *J. Surfactants Deterg*, **19**, 501 (2016).
49. L. Zhou, X. Jiang, Y. Li, Z. Chen and X. Hu, *Langmuir*, **23**, 11404 (2007).
50. C. C. Ren, F. Wang, Z. Q. Zhang, H. H. Nie, N. Li and M. Cui, *Colloids Surf. A*, **467**, 1 (2015).
51. R. Kamboj, S. Singh and V. Chauhan, *Colloids Surf. A*, **441**, 233 (2014).
52. S. M. Shaban, A. S. Fouda, M. A. Elmorsi, T. Fayed and O. Azazy, *J. Mol. Liq.*, **216**, 284 (2016).
53. X. F. Geng, X. Q. Hu, J. J. Xia and X. C. Jia, *Appl. Surf. Sci.*, **271**, 284 (2013).
54. I. Ahmad, P. Patial, C. Kaur and S. Kaur, *J. Surfactants Deterg*, **17**, 269 (2014).
55. V. Chauhan, S. Singh, R. Mishra and G. Kaur, *J. Colloid Interface Sci.*, **436**, 122 (2014).
56. D. Feng, Y. M. Zhang, Q. S. Chen, J. Y. Wang, B. Li and Y. J. Feng, *J. Surfactants Deterg*, **15**, 657 (2012).
57. M. El-Sukkary, N. Shaker, D. A. Ismail, S. M. Ahmed, M. Zaki and A. Awad, *Egyptian J. Pet.*, **21**, 37 (2012).
58. K. Taleb, M. Mohamed-Benkada, N. Benhamed, S. Saidi-Besbes, Y. Grohens and A. Derdour, *J. Mol. Liq.*, **241**, 81 (2017).
59. D. Q. Xu, X. Y. Ni, C. Y. Zhang, J. Mao and C. C. Song, *J. Mol. Liq.*, **240**, 542 (2017).
60. Y. Bao, J. J. Guo, J. Z. Ma, P. Liu, Q. L. Kang and J. Zhang, *J. Ind. Eng. Chem.*, **53**, 51 (2017).
61. N. A. Negm, A. S. El-Tabl, I. A. Aiad, K. Zakareya and A. H. Moustafa, *J. Surfactants Deterg*, **16**, 857 (2013).
62. M. Z. Mohamed, D. A. Ismail and A. S. Mohamed, *J. Surfactants Deterg*, **8**, 175 (2005).
63. H. L. Zhu, Z. Y. Hu, X. M. Ma, J. L. Wang and D. L. Cao, *J. Surfactants Deterg*, **19**, 265 (2016).
64. P. Gilbert and L. E. Moore, *J. Appl. Microbiol.*, **99**, 703 (2005).

65. J. Hao, T. Qin, Y. Zhang, Y. Li and Y. Zhang, *Colloids Surf. B Biointerfaces*, **181**, 814 (2019).
66. J. Haldar, P. Kondaiah and S. Bhattacharya, *J. Med. Chem.*, **48**, 3823 (2005).
67. S. M. Shaban, I. Aiad, A. H. Moustafa and O. H. Aljoboury, *J. Mol. Liq.*, **273**, 164 (2019).
68. A. B. Mirgorodskaya, E. I. Yackevich, D. R. Gabdrakhmanov, S. S. Lukashenko, Y. F. Zuev and L. Y. Zakharova, *J. Mol. Liq.*, **220**, 992 (2016).

Supporting Information

The influence of the Gemini surfactants hydrocarbon tail on in-situ synthesis of silver nanoparticles: Characterization, surface studies and biological performance

Samy M. Shaban[*,**,***] **and Dong-Hwan Kim**[*,**,†]

*School of Chemical Engineering, Sungkyunkwan University, Suwon 16419, Korea
**Biomedical Institute for Convergence at SKKU (BICS), Sungkyunkwan University, Suwon 16419, Korea
***Petrochemical Department, Egyptian Petroleum Research Institute (EPRI), Egypt
(*Received 19 December 2019 • accepted 13 March 2020*)

MATERIALS AND METHODS

1. Instrument Description

The chemical structures of the synthesized CACB, LACB, and PACB were confirmed using Fourier-transform infrared (FTIR). The benchtop 961, ATI Mattson Infinity series™ FTIR in-cooperated with Win First™ V2.01 software involved in the FTIR analysis (Egyptian Petroleum Research Institute, EPRI). Particle morphologies of the prepared AgNPs capped by the synthesized Gemini surfactants were examined using a Joel JeM - 2100 transmission electron

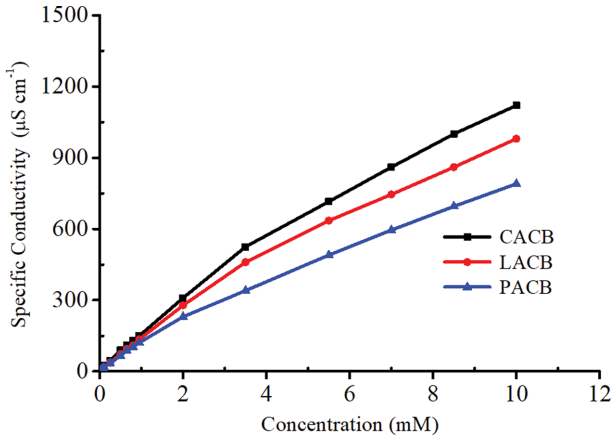


Fig. S1. Plots of specific electrical conductivity-concentration of prepared multi-electronic rich Gemini cationic amphiphilic in distilled water at 20 °C.

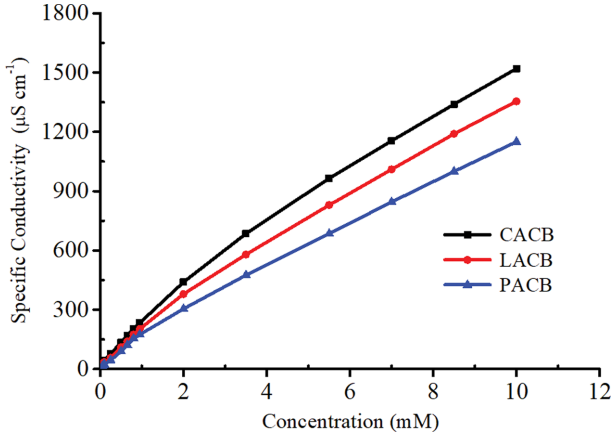


Fig. S2. Plots of specific electrical conductivity-concentration of prepared multi-electronic rich Gemini cationic amphiphilic in distilled water at 60 °C.

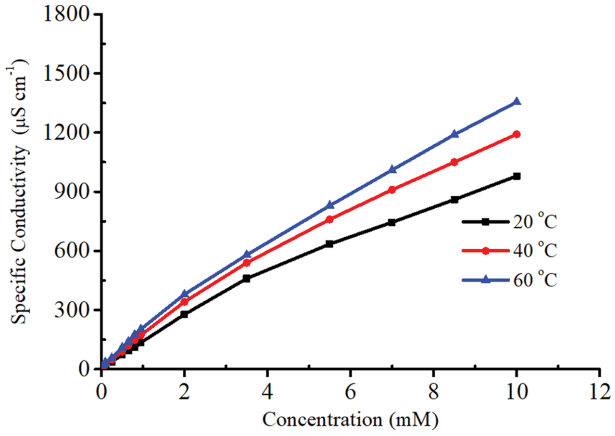


Fig. S3. Plots of specific electrical conductivity-concentration of LACB amphiphilic in distilled in distilled water at 20, 40, and 60 °C.

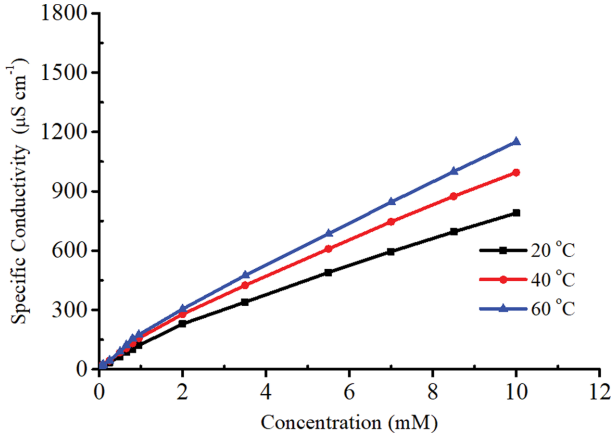


Fig. S4. Plots of specific electrical conductivity-concentration of PACB amphiphilic in distilled in distilled water at 20, 40, and 60 °C.

microscope (TEM) at EPRI. Few droplets of the synthesized AgNP colloids were droped onto a carbon-coated grid. The zeta potential & particle size distribution of the prepared AgNPs colloids were determined using a dynamic light scattering (DLS) technique (Malvern Zeta-sizer Nano device, Worcestershire, UK). Formation of AgNPs has been confirmed by UV-Vis spectroscopy performed on a double beam Shimadzu UV-2550 instrument (Japan).

RESULTS AND DISCUSSION

1. Specific Conductivity

The surfactants CACB, LACB, and PACB had a significant effect on solution conductivity. Figs. S1-S4 show the relationship between surfactant concentration and specific conductivity for CACB, LACB, and PACB at three different temperatures. The experimental results are based on increasing the solution specific conductivity with increasing surfactant concentration of CACB, LACB, and PACB, as shown in Figs. S1 and S2. These figures show that surfactant solution specific conductivity decreased with increasing hydrocarbon chain length. The specific conductivity also increased with increasing solution temperature, from 20 to 60 °C, as shown in Figs. S3 and S4, which outline the relationship between concentration of the synthesized surfactant and corresponding conductivity at 20, 40, and 60 °C.

2. Surface Tension (γ) Measurement

The critical micelle concentrations of CACB, LACB, and PACB in aqueous medium were assessed at 20, 40 & 60 °C, using γ measurements. Figs. S5-S7 illustrate the influence of increasing the hydrophobic double hydrocarbon tail on the surface tension of aqueous solutions. Increasing the hydrophobicity, free energy of solution increase, which forced the synthesized CACB, LACB, and PACB amphiphilic unimer to migration to the surface. As a result, additional reduction in surface tension is expected.

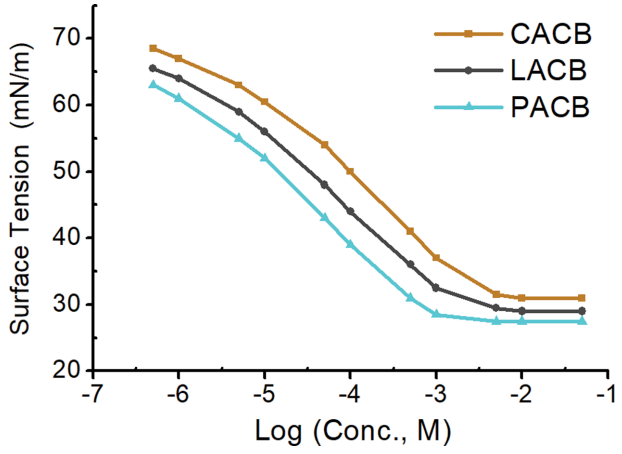


Fig. S5. The relationship between surface tension and log concentration of CACB, LACB, and PACB at 20 °C.

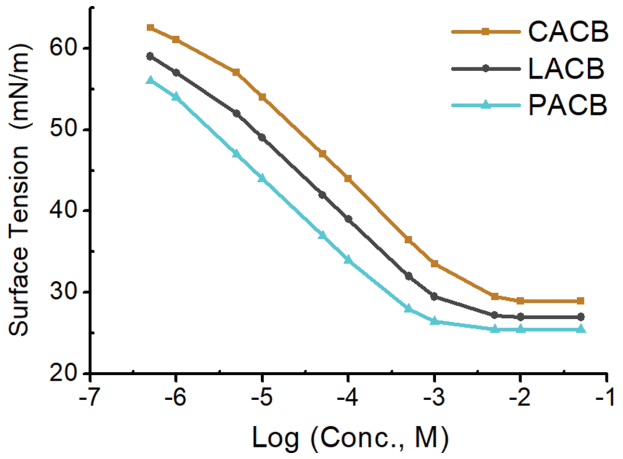


Fig. S6. The relationship between surface tension and log concentration of CACB, LACB, and PACB at 40 °C.

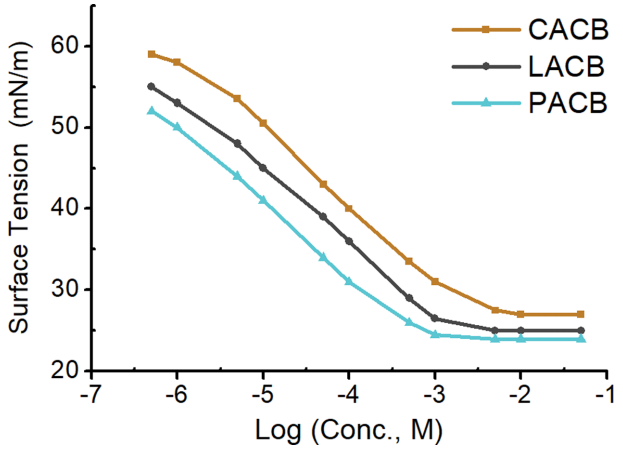


Fig. S7. The relationship between surface tension and log concentration of CACB, LACB, and PACB at 60 °C.